Am J Cancer Res 2023;13(9):3921-3940
www.ajcr.us /ISSN:2156-6976/ajcr0149612

Original Article

Cuproptosis-related lncRNAs as potential biomarkers of AML prognosis and the role of lncRNA HAGLR/miR-326/CDKN2A regulatory axis in AML

Ashuai Du[1*], Qinglong Yang[2*], Xinhua Luo[1]

[1]*Department of Infectious Diseases, Guizhou Provincial People's Hospital, Guiyang 550002, Guizhou, China;* [2]*Department of General Surgery, Guizhou Provincial People's Hospital, Guiyang 550002, Guizhou, China.* [*]*Equal contributors.*

Received February 11, 2023; Accepted May 19, 2023; Epub September 15, 2023; Published September 30, 2023

Abstract: Acute myeloblastic leukemia (AML) is the most prevalent form of AML in adults. Despite the availability of various treatment options, including radiotherapy and chemotherapy, many patients fail to respond to treatment or relapse. Copper is a necessary cofactor for all organisms; however, it turns toxic when concentrations reach a certain threshold maintained by homeostatic systems that have been conserved through evolution. However, the mechanism through which excess copper triggers cell death remains unknown. In this study, data on long non-coding RNAs (lncRNAs) related to cuproptosis were retrieved from publicly available databases. LASSO and univariate and multivariate Cox regression analyses were performed to establish an lncRNA model associated with cuproptosis specific to AML. To investigate the risk model, the Kaplan-Meier curve, principal component analysis, functional enrichment analysis, and nomographs were employed. The underlying clinicopathological characteristics were determined, and drug sensitivity predictions against the model were identified. Six cuproptosis-related lncRNA-based risk models were identified as the independent prognostic factors. By regrouping patients using a model-based method, we were able to more accurately differentiate patients according to their responses to immunotherapy. In addition, prospective compounds targeting AML subtypes have been identified. Using qRT-PCR, we examined the expression levels of six cuproptosis-associated lncRNAs in 30 clinical specimens. The cuproptosis-associated lncRNA risk-scoring model developed herein has implications in monitoring AML prognosis and in the clinical prediction of the response to immunotherapy. Furthermore, we identified and verified the ceRNA of the cuproptosis-related lncRNA HAGLR/miR-326/CDKN2A regulatory axis using bioinformatic tools. HAGLR is highly expressed in AML and AML cell lines. HAGLR inhibition significantly reduced the proliferation of AML cells and promoted apoptosis. Elesclomol promotes the degradation of CDKN2A and inhibits the proliferation of AML cells. Elesclomol combined with si-HAGLR inhibited the AML progression of AML both *in vitro* and *in vivo*.

Keywords: Acute myeloblastic leukemia, cuproptosis, HAGLR, miR-326, CDKN2A, elesclomol

Introduction

Acute myeloid leukemia (AML) is a type of hematopoietic cancer that results from aberrant proliferation and accumulation of leukemia cells (myeloid relatives) in the peripheral blood and bone marrow [1]. AML is the most prevalent form of adult acute leukemia and commonly emerges as a new malignancy with a very poor survival prognosis [2], especially in the elderly [3, 4]. Primary resistance to initial therapy and disease relapse remain significant challenges in the treatment of AML [5].

Copper is an essential cofactor for all organisms, and copper homeostasis is critical for a variety of physiological activities. Dysregulation of the intracellular bioavailability of copper can cause cytotoxicity and oxidative stress. Copper homeostasis is precisely maintained across the animal kingdom, from prokaryotes to eukaryotes, mostly by preventing excessive copper ion accumulation in cells, which threatens cell survival. Several pioneering studies have examined various forms of cell death, such as apoptosis [6], necroptosis [7], pyroptosis [8], and ferroptosis; however, few studies have focused

on cytotoxicity induced by excess levels of copper [9-11]. Several explanations have been proposed for the precise mechanisms by which copper ions cause cell death. These explanations include the initiation of apoptosis [12, 13], caspase-independent cell death [14], generation of reactive oxygen species (ROS) [15, 16], and suppression of the ubiquitin-proteasome system [17-19]. However, there has been no concensus on this topic. Therefore, the specific mechanisms underlying the effects of copper on cell death need to be further investigated.

The expression profiles of 19 cuproptosis genes and 55,187 long non-coding RNAs (lncRNAs) obtained from the dataset provided by The Cancer Genome Atlas (TCGA) were used in this investigation. Subsequently, Pearson's correlation analysis was used to detect cuproptosis-associated lncRNAs. This model was designed to examine the overall survival (OS) of patients with AML and was based on a novel cuproptosis gene prognostic model. Using a publicly accessible database of drug sensitivity, potential drug candidates targeting this lncRNA signature related to cuproptosis were identified. Furthermore, connections associated with immunotherapy responses were investigated. A nomogram was constructed to predict the OS of patients with AML. Finally, we investigated the expression profiles of cuproptosis-related lncRNAs and verified their potential regulatory mechanisms in AML.

Materials and methods

Data collection of patients with AML

Using the VarScan program, we acquired RNA-seq transcriptomic data, associated clinical data, and variant data from TCGA databases for patients with AML.

Selection of cuproptosis genes and cuproptosis-associated lncRNAs

Our team acquired lncRNAs and cuproptosis genes from TCGA database. Based on earlier investigations, the expression matrix of 19 cuproptosis genes, including NFE2L2, NLRP3, ATP7B, ATP7A, SLC31A1, FDX1, LIPT1, LIAS, LIPT2, DLAT, DLD, PDHA1, MTF1, PDHB, GLS, DBT, CDKN2A, GCSH, and DLST, was also retrieved from TCGA database. We selected cuproptosis-associated lncRNAs via Pearson's correlation analysis and identified 1255 cuproptosis-associated lncRNAs. The criteria used for this procedure was |Pearson R| > 0.4 and $P < 0.001$.

Construction and verification of the risk signature

We first integrated the data from TCGA databases, performed batch correction to reduce variance, and obtained the joint database. The complete TCGA dataset was divided into training and testing sets using a random process. The training set was employed to develop the cuproptosis-associated lncRNA model, and TCGA full and test sets were used to verify the constructed model. None of the datasets exhibited significant differences in the performance of patients in the clinic ($P > 0.05$). Combining information on AML survival from TCGA databases, our team selected the prognostic results from 1255 cuproptosis-associated lncRNAs in TCGA datasets, and univariate Cox regression analyses were utilized. Using the R package glmnet for LASSO Cox regression analyses (via penalized parameters speculated by 10-fold cross-verification) in TCGA datasets, 18 lncRNAs related to cuproptosis were found to be correlated with OS in patients with AML. Multifactorial Cox regression analyses were used to analyze these 18 cuproptosis-associated lncRNAs, resulting in six cuproptosis-associated lncRNA risk models. Subgroups such as high- and low-risk groups were created according to the mid-value of the risk score.

Function analysis

Our team completed Gene Ontology (GO) and KEGG analyses to determine DEGs, which used the R package clusterProfiler. The analytical liminal value was identified using the *P*-value, with $P < 0.05$, indicating significant functional annotation enrichment.

Tumor mutation and drug susceptibility analysis

The R package "maftools" was employed to transform somatic mutation files obtained from TCGA database into a mutation annotation format, and the mutation status of specimens from both high-risk and low-risk cohorts was inspected. Furthermore, tumor mutation bur-

den (TMB) scores were computed for each risk group, and the relationship between tumor mutation burden (TMB) scores and the respective risk scores was examined. Compounds associated with the clinical treatment of AML were identified by calculating the semi-inhibitory concentrations (IC50) for the AML dataset, which was acquired from the Cancer Drug Sensitivity Site (GDSC) in the TCGA project. The IC50 values of these compounds were determined using the R package (pRRophetic).

Principal component analysis (PCA) and Kaplan-Meier survival curve analysis

PCA was utilized for efficient reduction of dimensions, recognition of models, and visualization of high-dimensional data in groups, including complete profiles of genetic expression, 19 cuproptosis genes, 1255 cuproptosis-associated lncRNAs, and risk models based on the expression patterns of six cuproptosis-related lncRNAs. Our team employed KM survival analyses to evaluate OS diversity between the low-risk and high-risk groups. The R packages survival and survMiner were used for such analyses.

Establishing and proving a prognostic factor

The predictive power of the independent prognostic factors (age, sex, grade, stage, and risk scoring) for 1-, 3-, and 5-year OS was established. Based on the Hosmer-Lemeshow test, calibration curves were used to demonstrate the concordance between the actual and anticipated model outcomes.

Extraction of RNA, qRT-PCR, and reverse transcription

Plasma samples were collected from 30 patients with AML and healthy donors (NC). This study was approved by the Ethics Committee of our hospital. Total RNA from lineage cells and AML and NC plasma samples was prepared using TRIzol reagent (Invitrogen) or the QIAGEN FFPE RNeasy kit (QIAGEN). Total RNA was prepared using the RevertAid First-Strand cDNA Prep Tool (Thermo Fisher Scientific, USA) to convert the RNA into cDNA by reverse transcription. Gene expression was normalized to that of GAPDH. For quantitative real-time PCR experiments, FastStart Universal SYBR Green Master Mix (Roche) was used with StepOne (Applied Biosystems, USA). The relative fold changes in expression were analyzed via the $2^{-\Delta\Delta CT}$ approach. The following primer sequences were as follows: AL590705.3 forward 5'-CCTTTGGTAGAAGCTCCTGTCT-3', and reverse 5'-TTTCCTTGGCAGAACCACAA-3'; LINC01094 forward 5'-CAAACCAGTTGTGCAGAGCC-3', and reverse 5'-GCTCTTGGCAAGCAACACTC-3'; AC147067.2 forward 5'-CTTCCCTTATCACCGTTAGCCA-3', and reverse 5'-CACAGTTGCACAGACGACA-3'; AC023511.1 forward 5'-TGGCTCAACACAATGCCCAA-3', and reverse 5'-TTTATGTGTGGCCCCAGAAGG-3'; AC016394.2 forward 5'-GGTAAGACGGACGCCAGATT-3', and reverse 5'-GTAAGTAACGCCGGCATGTG-3'; HAGLR forward 5'-TGCTGCATGACACGTACTCC-3', and reverse 5'-GGAAGAGCCAAGTCAGACGA-3'; CDKN2A forward 5'-CCGTGGACCTGGCTGAGGAG-3', and reverse 5'-CGGGGATGTCTGAGGGACCTTC-3'; GAPDH forward 5'-GGACGCATTGGTCGTCTGG-3', and reverse 5'-TTTGCACTGGTACGTGTTGAT-3'; miR-326 mimic TATCCTCTGGGCCCTTCCT.

Cell culture

AML cell lines (Kasumi-1, MOLM13, HL-60, and THP-1) and GM12878 were obtained from the ATCC (ATCC, Manassas, VA, USA). AML cells were cultured in RPMI-1640 medium (Hyclone; GE Healthcare) and stored in a humidified incubator at 37°C under 5% CO_2.

Cell proliferation

AML cells were cultured in 96-well plates (2×10^5 cells/well). After incubation at 37°C under 5% CO_2 for different time periods, 10 μL CCK-8 (Dojindo, Kumamoto, Japan) was added to the cells, and cell were maintained for another 4 h. A microplate reader (Potenov, Beijing, China) was used to measure the absorbance at 450 nm.

Cell apoptosis assay

Apoptosis was measured using an Apoptosis Detection Kit (Sigma-Aldrich). AML cells (2×10^5 AML cells per well) were seeded into 12-well plates. After 24 h of treatment, the cells were collected and treated with Annexin V-binding buffer, followed by labeling with Annexin V-FITC and PI (Sigma). The percentage of apoptotic cells was assessed using flow cytometry.

Dual-luciferase assay

The online tool TargetScan was used to identify the potential binding sites. The wild-type (wt) and mutant (mut) sites of HAGLR (HAGLR wt and HAGLR mut) and CDKN2A (CDKN2A wt and CDKN2A mut), including the homologous binding sites of miR-326, were amplified and uniformly cloned into the vector pGL3 (Promega). The dual-luciferase reporter assay system (Promega) was used to detect luciferase activity.

Western blotting

RIPA lysis buffer (Beyotime, Shanghai, China) was used to extract proteins from the AML cells. Western blotting was used to determine the expression levels of the proteins involved in this study as previously described. The membrane was incubated with CDKN2A (1:1000, Abcam, UK) and β-actin (1:3000, Abcam, UK) overnight at 4°C. Horseradish peroxidase-conjugated goat anti-rabbit secondary antibodies (1:5000; Abcam) were also used. Finally, an ECL detection kit (Beyotime) was used to visualize the protein signals on the membrane.

Tumor transplantation in nude mice

Mice aged 4-6 weeks were fed in a specific pathogen animal laboratory for 1 week. The mice were randomly divided into four groups containing three mice each. A cell suspension (0.1 mL; 1×10^6) was prepared from HL-60 cells of different treatments and injected subcutaneously into the neck and back. When the tumor volume reached approximately 100 mm^3, the animals were randomly divided into four groups: saline, si-HAGLR, elesclomol, and si-HAGLR+elesclomol (n = 3 mice per group).

Different formulations of si-HAGLR (20 mg siRNA per mouse equivalent) and elesclomol (30 mg/kg per mouse equivalent) were administred as a treatment via tail vein injection once a week. On day 28, all animals were euthanized, and the following formula was used to quantify tumor volume: V (volume) = (length width^2)/2; extracted and imaged tumor tissue. Finally, the tumors were extracted for histopathological analysis.

Hematoxylin and eosin (H&E) staining

Using a microtome, 4 μm sections were obtained from each paraffin block. The sections were immersed in xylene for 10 min, rehydrated with absolute ethanol and 95%, 85%, and 70% ethanol in turn for 5 min, immersed, and washed with PBS solution for 3 times for 5 min each. Next, 100 μL of pre-prepared hematoxylin solution was added to each tissue section and allowed to stain for 10 min. The sections were subsequently stained with an eosin solution for 3 min, dehydrated with graded alcohol, and cleared in xylene. Finally, the slides were mounted using neutral resin.

Immunohistochemistry (IHC)

The tissues from nude mice were cut into 4 μm slides. Ki-67 and CDKN2A antibody were purchased from Cell Signaling Technology. The IHC analysis was performed as described previously [20]. Images were observed under a microscope (Olympus, Tokyo, Japan) at appropriate magnification.

Statistical analysis

One-way analysis of variance (ANOVA) and paired sample *t*-tests were used to assess differences between groups. Pearson's correlation test was used to analyze the correlations. Statistical analyses were performed using SPSS 23.0 and GraphPad Prism 7.0.1 softwares. All experiments were performed independently and repeated thrice. Statistical significance was set at $P < 0.05$.

Results

Identification of cuproptosis-associated lncRNAs in patients with AML

The workflow for the risk model construction and subsequent analyses is shown in Supplementary Figure 1. TCGA database was used to extract 55,187 lncRNAs and 19 cuproptotic genes. LncRNAs related to cuproptosis were classified as lncRNAs connected to one or more of the 19 cuproptosis genes (|Pearson R| > 0.3 and $P < 0.001$). **Figure 1A** depicts the co-expression of the cuproptosis-lncRNA network as a Sankey diagram and identifies cuproptosis-associated lncRNAs. **Figure 1B** shows the relationship between cuproptosis genes and

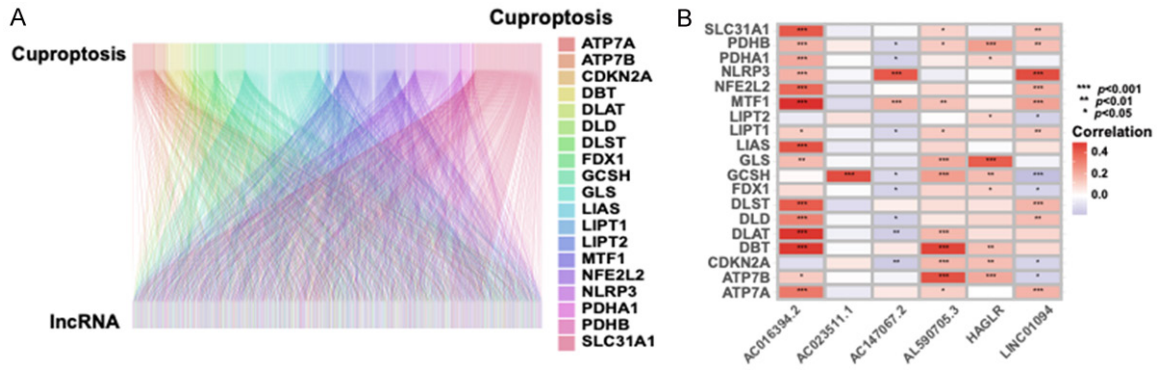

Figure 1. Determination of Cuproptosis-associated lncRNAs in AML sufferers. A. Sankey relation chart for cuproptosis genes and cuproptosis-associated lncRNAs. B. Heat map for the association between cuproptosis genes and the 6 prognosis cuproptosis-associated lncRNAs.

cuproptosis-associated lncRNAs in TCGA dataset.

Construction and validation of a risk model for patients with AML based on lncRNAs related to cuproptosis

Univariate Cox regression analysis was utilized in the training set to identify cuproptosis-associated lncRNAs related to AML prognosis among 1255 cuproptosis-associated lncRNAs identified from all three databases. We found that 16 cuproptosis-associated lncRNAs in TCGA were correlated with OS in patients with AML (Supplementary Figure 2A). Lasso-penalized Cox analyses are prevalent multi-regression analyses, the use of which not only increases the predicted interpretability and accuracy of statistical models, but also permits simultaneous variate selection and regularization. This approach is widely used for the optimal selection of features with low correlations and prominent predictive values in high-dimensional data to avoid overfitting. Therefore, this approach can help to validate the most predictive biomarkers and generate prognostic indices for determining clinical outcomes. LASSO analysis was implemented to extract potential 16 cuproptosis-associated lncRNA signatures for prognostic prediction in patients with AML. The cvFIT output and lambda curves are shown in Supplementary Figure 2B and 2C. The high- and low-risk groups were classified based on the median risk score, which showed a stronger ability to predict patient survival than traditional clinicopathological features. The risk score for each sample was obtained using the prognostic model formula. The sample was divided into high-risk (N = 199) and low-risk (N = 171) groups. **Figure 2A** depicts the distribution of risk scores in the high- and low-risk groups in the entire cohort, whereas **Figure 2B** depicts the survival times of patients between the groups in the whole cohort. Heat maps illustrate the expression of the six cuproptosis-related lncRNA signatures in the high- and low-risk groups of the entire cohort (**Figure 2C**). Survival analyses revealed a higher OS in the low-risk group than in the high-risk group in the entire cohort ($P < 0.001$; **Figure 2D**). To evaluate the predictive accuracy of this well-established model in the test and training groups, risk scores were generated for each patient by using a standard formula. The test group was divided into high-risk (N = 106) and low-risk (N = 78) groups. The training group was divided into high-risk (N = 93) and low-risk (N = 93) groups. **Figure 3** illustrates the risk grades distribution, survival time and status patterns, and expression of cuproptosis-associated lncRNAs in the test group (**Figure 3A-C**) and training group (**Figure 3E-G**). Kaplan-Meier curves revealed that the OS ratio of the AML samples in the low-risk group was significantly higher than that in the high-risk group in the test and training groups (**Figure 3D** and **3H**).

Principal-component analysis (PCA) verified the grouping ability of the cuproptosis-related lncRNA model

PCA was conducted to examine the difference between groups with low- and high-risk depending on complete gene expression, 19 cuproptosis genes, six cuproptosis-associated lncRNAs, and a model of risk classification based on the

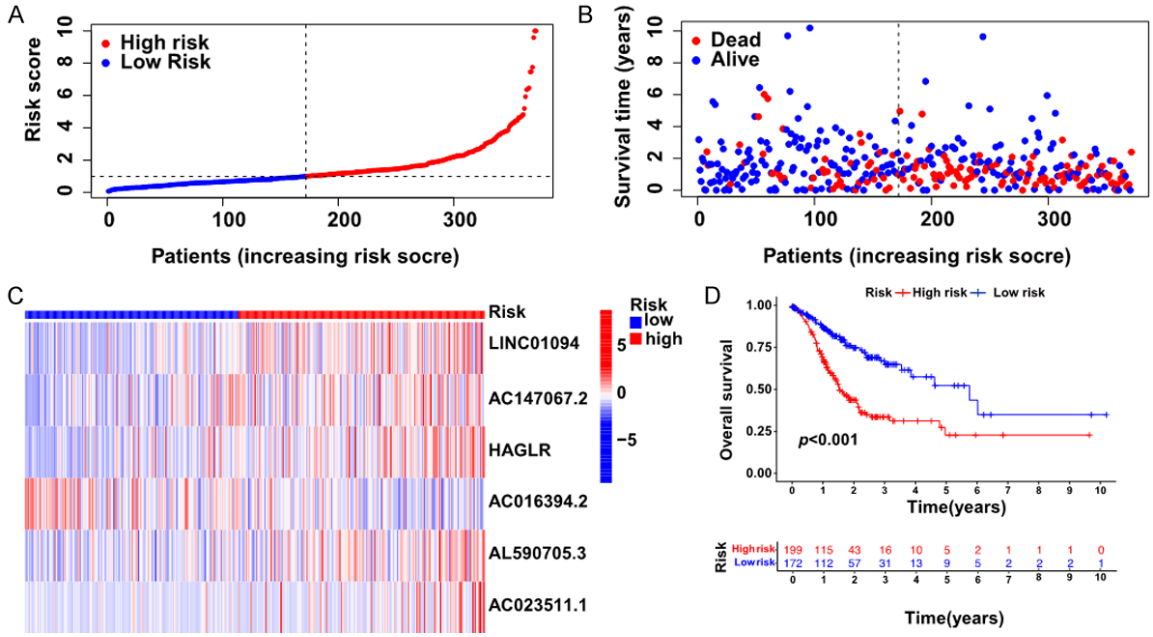

Figure 2. The risk patterns' prognostic value of the 6 cuproptosis-asociated lncRNAs in the TCGA entire sets. A. Risk score distribution based on the lncRNA model associated with cuproptosis. B. Different survival time patterns between the groups with high- and low-risk. C. The expression levels of the six prognostic lncRNAs are shown in a heatmap for each patient using clustering analysis. D. The KM survival curves for both high- and low-risk patients.

expression profiles of six cuproptosis-associated lncRNAs (Supplementary Figure 3A-D). As shown in Supplementary Figure 3A-C, the distribution of both risk groups was comparatively dispersed. Conversely, based on the findings of our model, the low- and high-risk groups exhibited distinct distributions (Supplementary Figure 3D). Based on these findings, it appears that prognostic characteristics can differentiate between low- and high-risk groups.

Estimation of the tumor immune microenvironment and cancer immunotherapy response using the cuproptosis-associated lncRNA model

To explore the relationship between the risk model and the immune status, we quantified the enrichment scores of diverse immune cell subpopulations, associated functions, and pathways using ssGSEA. The contents of the antigen presentation process, including the score of T cell co-stimulation, antigen presenting cell (APC) co-stimulation, inflammation-promotion, and MHC class I, were significantly different between the high-risk and low-risk groups. Moreover, the scores for T cell co-inhibition, APC co-inhibition, inflammation promotion, type I IFN response, and type II IFN response were higher in the high-risk group (**Figure 4A**). GO analysis showed that cuproptosis-related lncRNAs were enriched in skeletal system development, pattern specification, and anterior/posterior pattern specification (**Figure 4B**). KEGG analysis showed that these cuproptosis-related lncRNAs may be related to cytokine-cytokine receptor interactions, Malaria, and PI3K-Akt signaling pathways, suggesting that these lncRNAs are involved in tumor development (**Figure 4C**). In addition, differences in sensitivity to immunotherapy between patients in the high- and low-risk groups were investigated using the TIDE algorithm (http://tide.dfci.harvard.edu/). The TIDE algorithm develops a recently developed tool for evaluating the effectiveness of immune checkpoint therapies for tumors [21]. In this study, the TIDE score in the high-risk group was higher than that in the low-risk group (**Figure 4D**). Nevertheless, further investigation is essential to determine whether immunotherapy is more advantageous for patients with AML in the low-risk group than those in the high-risk group. Next, we used the maftools algorithm to observe mutations in the high- and low-risk groups and showed that for most genes, the frequency of mutations was higher

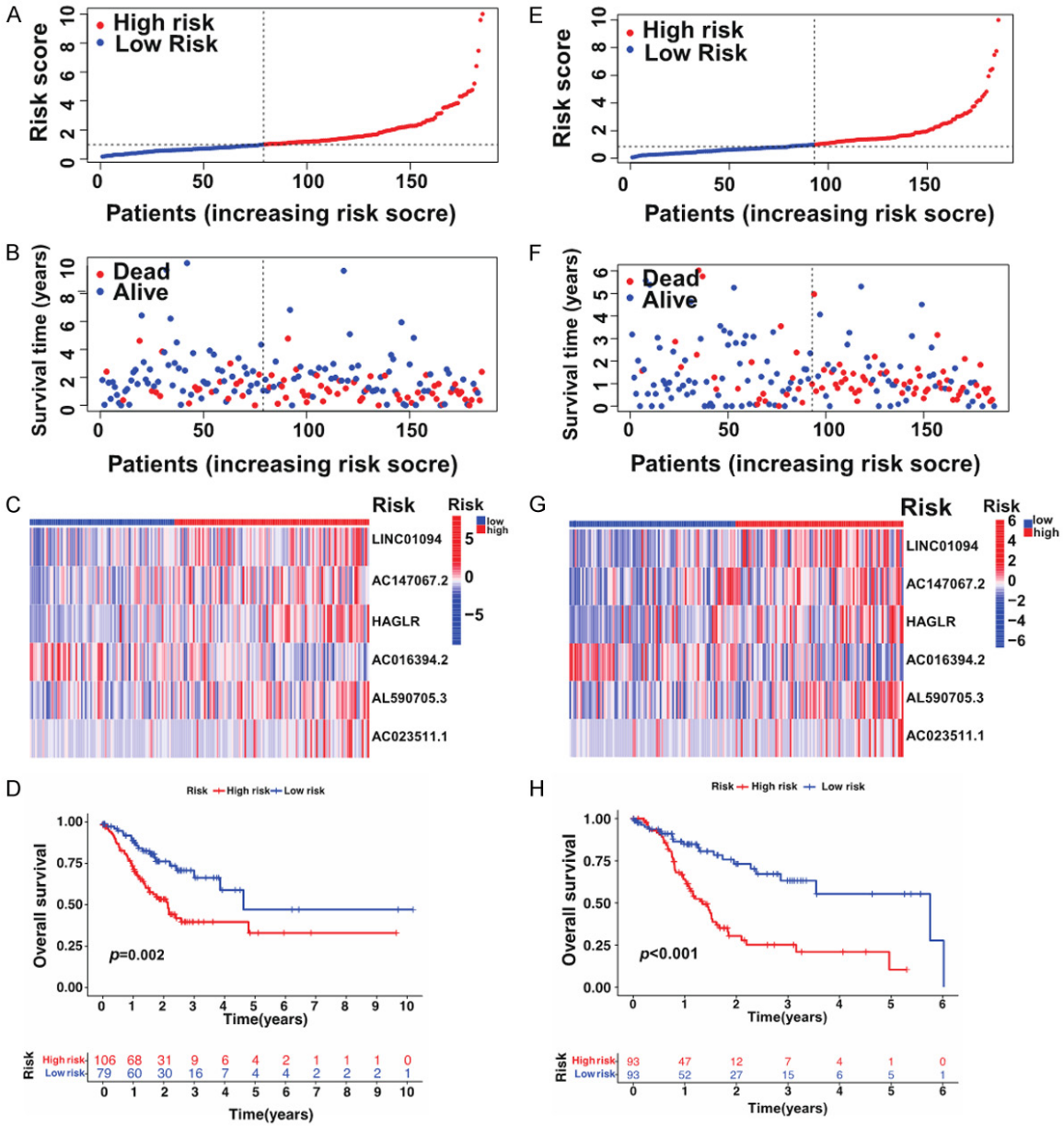

Figure 3. The risk patterns' prognostic value of the 6 cuproptosis-asociated lncRNAs in the TCGA testing and training set. A. The risk score distribution based on the lncRNA model associated with cuproptosis in the test set. B. Survival status and time patterns of the high- and low-risk groups. C. Heatmap derived from the clustering analysis depicting the expression levels of six prognostic lncRNAs for each patient. D. KM survival curves of patients in both groups. E. Distribution of risk scores based on the lncRNA model associated with cuproptosis in the training set. F. Survival status and time patterns of the low- and high-risk groups. G. Heatmap derived from the clustering analysis depicting the expression levels of six prognostic lncRNAs for each patient. H. KM survival curves for both high- and low-risk patients.

in the low-risk group than in the high-risk group (*TTN*: low-risk, 57%; high-risk, 45%; *TP53*: low-risk, 39%; high-risk, 45%; *MUC16*: low-risk, 36%; high-risk, 25%) (**Figure 4E**, **4F**). The difference in TMB between the high- and low-risk groups was significant ($P = 0.0014$; **Figure 4G**).

We further investigated the probable differences in survival between patients with high and low TMB. A significant survival advantage was observed in the high-TMB group compared with the low-TMB group ($P = 0.020$; **Figure 4H**), whereas patients in the in the low-TMB and low-

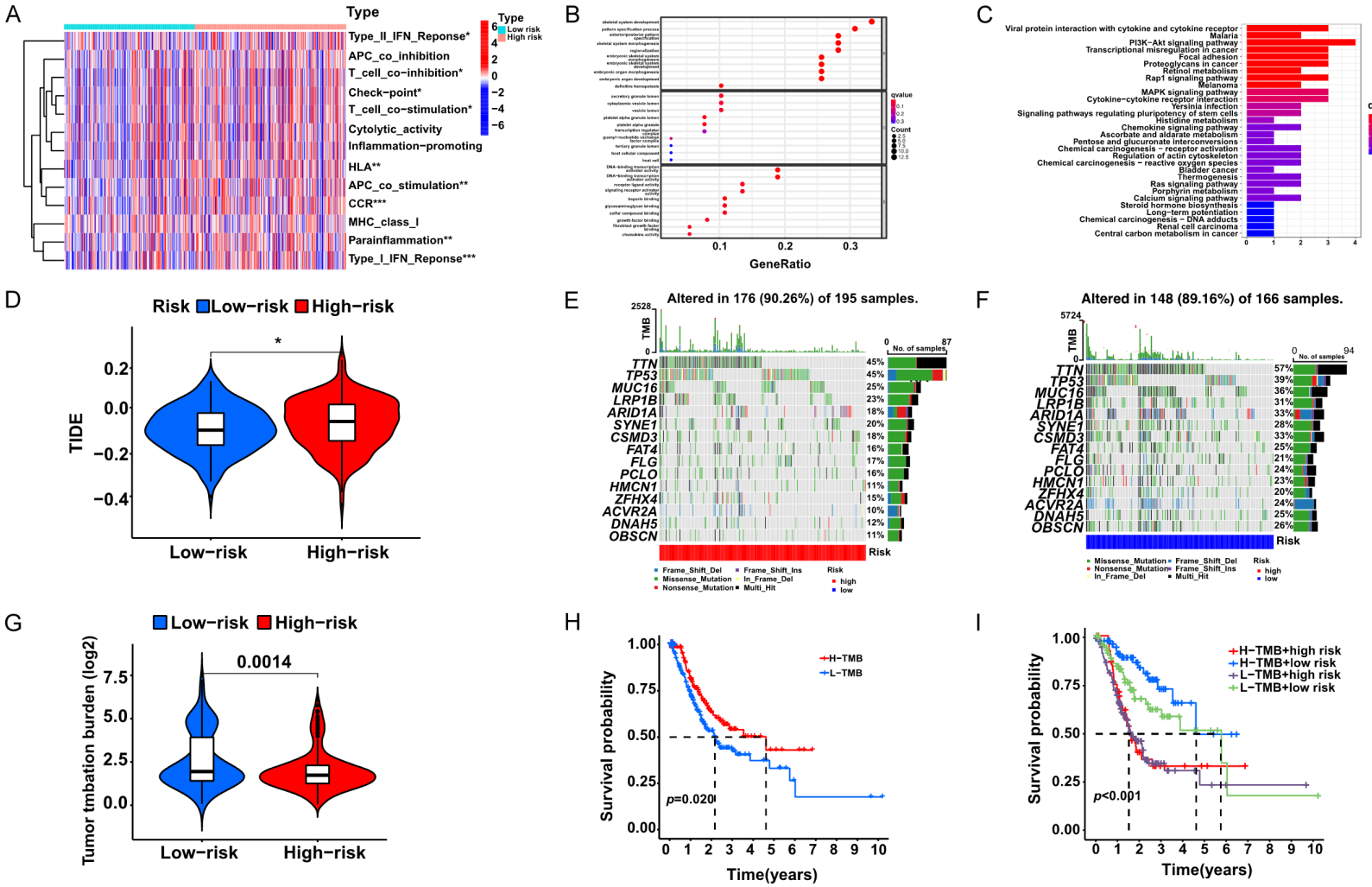

Figure 4. Evaluation of the cancer immunotherapy response and tumor immune microenvironment employing the lncRNA model related to Cuproptosis-in the TCGA entire set. (A) The indicated criteria of the immune indicator for every sufferer. (B) GO enrichment analyses. (C) KEGG enrichment analyses. (D) The difference in TIDE prediction between patients at high- and low-risk. (E and F) The water fall plot presents variant data of the genes with great variant frequencies in the group with high-risk (E) and the group with low-risk (F). (G) TMB diversity within the low-risk group and high-risk group. (H) Survival analysis using K-M curves for the groups with high TMB and low TMB (P = 0.020, log-rank test). (I) Survival analysis for sufferers categorized by high- and low-risk group and TMB via K-M curves (P < 0.001, log-rank test).

risk groups had a more remarkable survival advantage ($P < 0.001$; **Figure 4I**). These findings indicate that low- or high-risk can be used to evaluate the clinical prognoses of patients with AML.

Identification of novel candidate compounds targeting the cuproptosis-associated lncRNA model

The pRRophetic algorithm was utilized to evaluate the treatment activity, depending on the IC50 that was present in the GDSC database, for every sample to detect potential drugs targeting the lncRNA model that could be used to treat patients with AML. We observed that 56 compounds were evaluated for significant variation between these groups in terms of the calculated IC50, and all of these compounds were more sensitive to the high group. Supplementary Figure 4 illustrates the top 19 compounds that can be used for further investigation in patients with AML.

Investigation of the cuproptosis-associated lncRNA prognostic risk model and clinical characteristics of AML

Univariate and multivariate Cox regression analyses were conducted to determine whether risk modeling was an independent prognostic factor for AML. The risk scoring hazard ratio (HR) and 95% confidence interval (CI) were 1.13 and 1.07-1.19 ($P < 0.001$; **Figure 5A**), respectively, in a univariate Cox regression analysis. The HR and 95% CI in the univariate Cox regression analysis were 1.14 and 1.08-1.20, respectively ($P < 0.001$; **Figure 5B**), demonstrating that risk modeling has the potential to be an independent prognostic factor. In contrast to clinical variables, the risk modeling of prognostic factors predominantly presented predictive utility in the nomogram analysis (**Figure 5C**). The consistency indicator of risk scoring and area under the receiver operating characteristic (ROC) curve (AUC) were investigated to further assess the sensitivity and uniqueness of risk scoring for AML prognosis. The consistency of the risk scoring index was consistently higher than that of other clinical factors over time, suggesting that risk scoring was superior for AML prognosis (**Figure 5D**). The predicted one-, three-, and 5-year OS rates showed satisfactory coherence (**Figure 5E**). Subsequently, ROC curves with time dependence were employed to investigate the prognostic power of the risk class, age, and sex from TCGA database. The AUC of the risk score was 0.703, which was better than that of age (0.594), sex (0.522), and stage (0.561) (**Figure 5F**), indicating that risk modeling based on the six cuproptosis-associated lncRNAs is more reliable. Similarly, the AUCs for OS at one, three, and five years were 0.703, 0.722, and 0.680, respectively, in all groups (**Figure 5G**), indicating that the signature was reliable and could be effectively applied in clinical practice.

lncRNA HAGLR mainly locate in the cytoplasm and its knockdown inhibits AML cell proliferation and promote apoptosis

We conducted qRT-PCR to assess lncRNAs in the peripheral blood samples of patients with AML and NC and found that the expression of HAGLR was significantly upregulated in patients with AML compared to other lncRNAs (**Figure 6A**). Compared to the NC, the expression of HAGLR was significantly upregulated in AML samples (**Figure 6B**). In AML cell lines, the expression of HAGLR were significantly upregulated in THP-1 and HL-60 compared to that in AML cell lines (**Figure 6C**). Functional interference techniques were used to evaluate the behavioral effects of HAGLR deletion. **Figure 6D** shows that transfection was successful in the AML cell lines. siRNA#2 was selected for further experiments because it exerted the strongest inhibitory effect. The CCK-8 assay suggested that HAGLR knockdown significantly inhibited the proliferation of HL-60 and THP-1 cells (**Figure 6E**). The results of the FISH assay confirmed the localization of HAGLR in the cytoplasm (**Figure 6F**). Flow cytometric analysis demonstrated that HAGLR knockdown increased the proportion of apoptotic AML cells (**Figure 6G**). These findings demonstrate that the knockdown of HAGLR inhibits AML proliferation and promotes apoptosis *in vitro*, demonstrating that HAGLR plays a key role in stimulating the progression of AML.

miR-326 is sponged by lncRNA HAGLR

To further explore the specific mechanism of HAGLR as a ceRNA in AML, we identified the target miRNAs using the Mircode database (**Figure 7A**), and top 8 candidate miRNAs were screened to determine whether HAGLR might have spongy miRNAs in AML cells. We designed

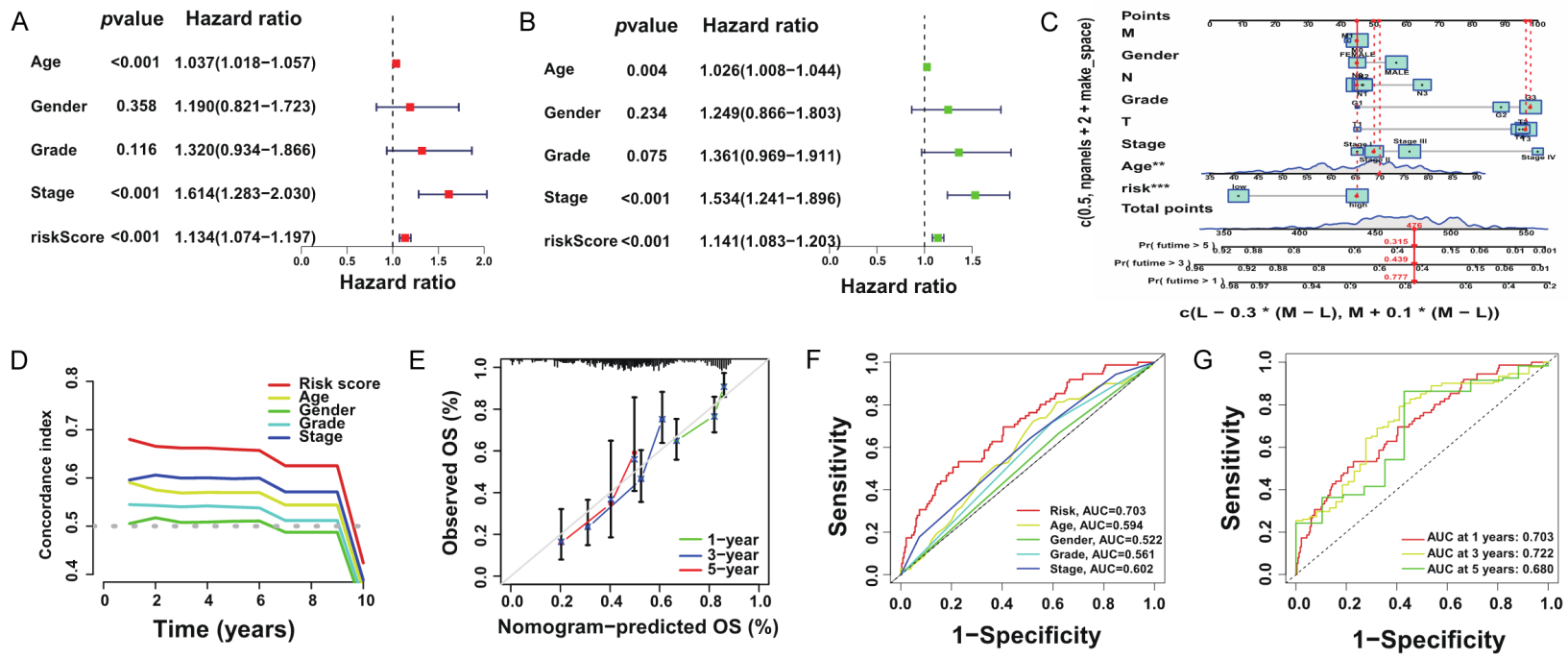

Figure 5. Evaluation of the prognosis risk modeling of the Cuproptosis-associated lncRNAs and clinic characteristics in AML in the TCGA entire set. A, B. Univariable and multivariable analysis of the clinic features and risk scoring with the OS. C. Nomograph on the foundation of sex, age, stage, grade, and risk scoring. D. Concordance indicators of the risk scoring and clinic features. E. The correction plot of the nomograph forecasts the possibility of the 1-, 3-, and 5-years OS. F. ROC curves of the clinic features and risk scoring. G. ROC curves for the risk scoring within the TCGA entire set (to forecast 1, 3, and 5-year OS).

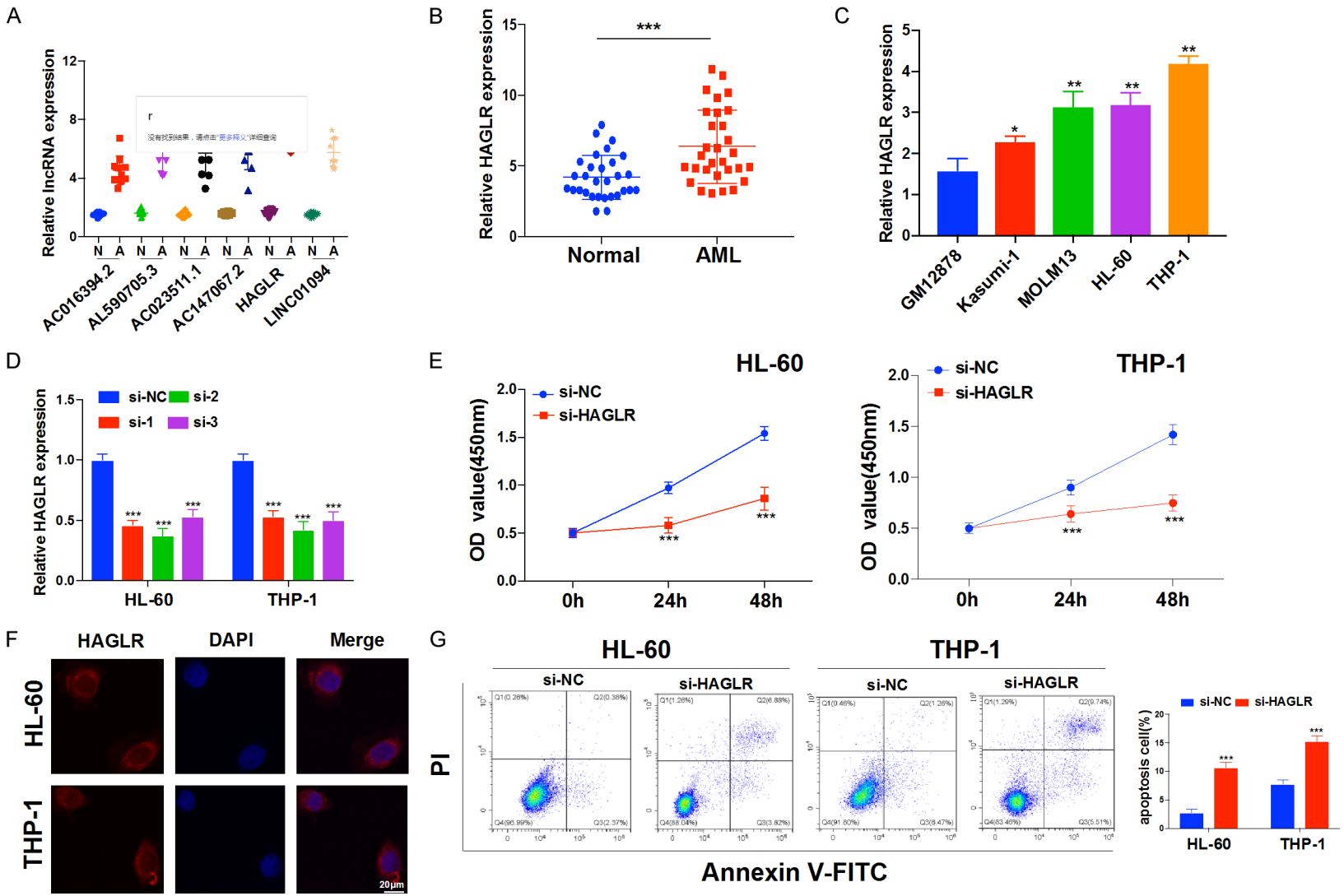

Figure 6. Cuproptosis-associated lncRNAs HAGLR promotes cell proliferation and inhibits apoptosis in AML. A. The expression of 10 lncRNAs expression in blood samples from patients with AML. B. The level of HAGLR in the blood samples from 30 AML sufferers and matched healthy control was examined with qRT-PCR analysis. C. The level of HAGLR in GM12878, Kasumi-1, MOLM13, HL-60, and THP-1 cells was determined by qRT-PCR assay. D. The efficiency of HAGLR knockdown (si-HAGLR-1, si-HAGLR-2, and si-HAGLR-3) was assessed by qRT-PCR. E. The proliferation of HL-60 and THP-1 cells was detected by CCK-8 assays. F. The results of FISH assay also confirmed that HAGLR was colocalized in the cytoplasm. Scale bars are 20 μm. G. Cell apoptosis analysis of AML cells with si-HAGLR-2. Data are shown as the mean ± standard deviation of three independent experiments. *$P < 0.05$; **$P < 0.01$; ***$P < 0.001$.

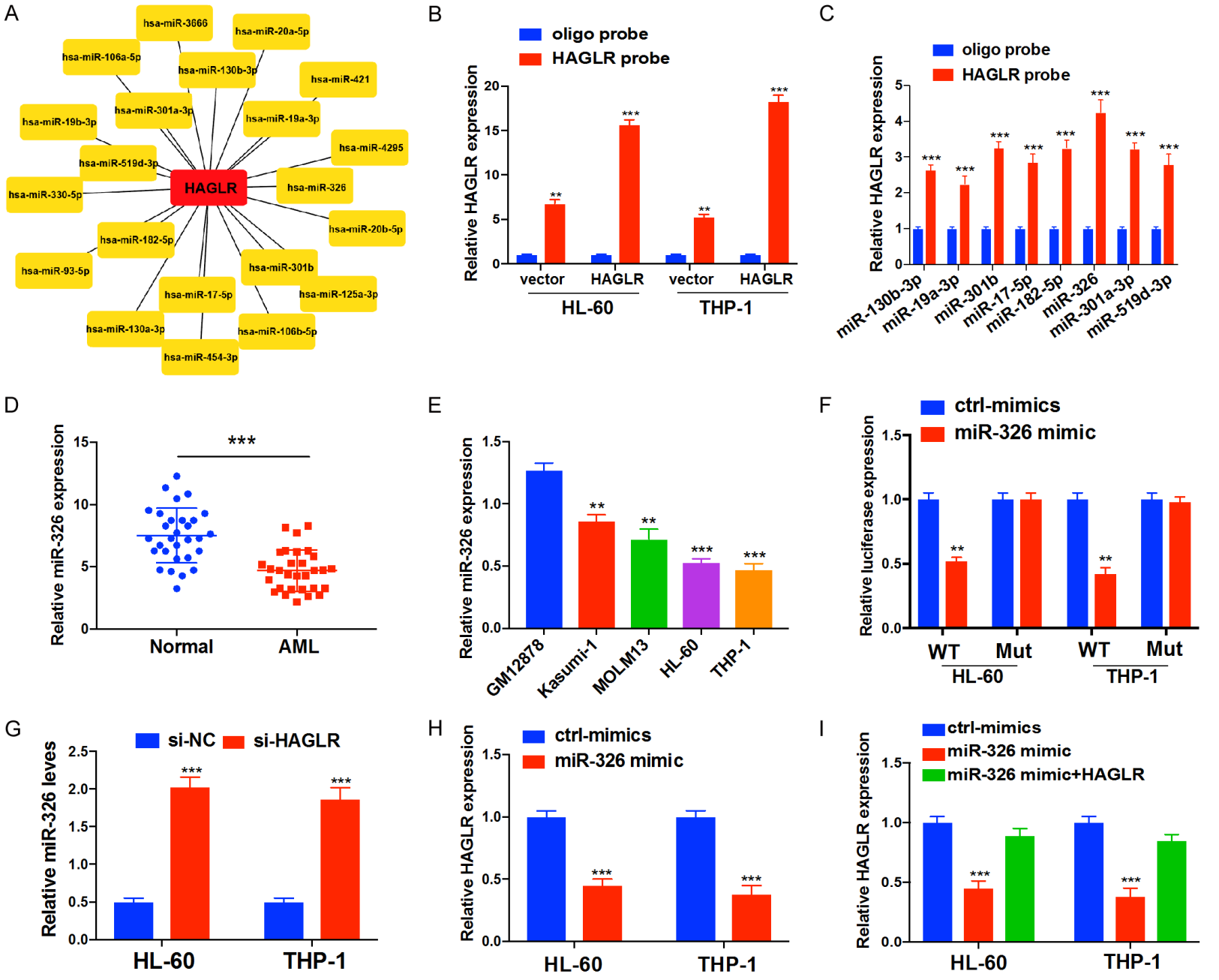
A
hsa-miR-3666
hsa-miR-20a-5p
hsa-miR-106a-5p
hsa-miR-130b-3p
hsa-miR-421
hsa-miR-19b-3p
hsa-miR-301a-3p
hsa-miR-19a-3p
hsa-miR-4295
hsa-miR-519d-3p
HAGLR
hsa-miR-330-5p
hsa-miR-326
hsa-miR-20b-5p
hsa-miR-182-5p
hsa-miR-93-5p
hsa-miR-301b
hsa-miR-17-5p
hsa-miR-125a-3p
hsa-miR-130a-3p
hsa-miR-106b-5p
hsa-miR-454-3p
B
oligo probe
HAGLR probe
Relative HAGLR expression
vector
HAGLR
vector
HAGLR
HL-60
THP-1
C
oligo probe
HAGLR probe
Relative HAGLR expression
miR-130b-3p
miR-19a-3p
miR-301b
miR-17-5p
miR-182-5p
miR-326
miR-301a-3p
miR-519d-3p
D
Relative miR-326 expression
Normal
AML
E
Relative miR-326 expression
GM12878
Kasumi-1
MOLM13
HL-60
THP-1
F
ctrl-mimics
miR-326 mimic
Relative luciferase expression
WT
Mut
WT
Mut
HL-60
THP-1
G
si-NC
si-HAGLR
Relative miR-326 leves
HL-60
THP-1
H
ctrl-mimics
miR-326 mimic
Relative HAGLR expression
HL-60
THP-1
I
ctrl-mimics
miR-326 mimic
miR-326 mimic+HAGLR
Relative HAGLR expression
HL-60
THP-1

Figure 7. lncRNA HAGLR acted as ceRNA for miR-326. A. Schematic diagram of target miRNA of HAGLR. B. The pull-down efficiency of biotinylated HAGLR probe tested by qRT-PCR in HL-60 and THP-1 cells. C. The comparative levels of 8 miRNA candidates in AML cells were detected by qRT-PCR. D. The level of miR-326 in the blood samples from 30 AML sufferers and matched healthy control was examined with qRT-PCR analysis. E. The level of miR-326 in GM12878, Kasumi-1, MOLM13, HL-60 and THP-1 cells was determined by qRT-PCR assay. F. The relationship between HAGLR and miR-326 in HL-60 and THP-1 cells was performed by dual-luciferase reporter assay. G. miR-326 expression following si-HAGLR transfection was assessed by qRT-PCR. H. HAGLR expression following miR-326 overexpression was measured by qRT-PCR. I. HAGLR expression following HAGLR overexpression and miR-326 mimic was assessed by qRT-PCR. Data are shown as the mean ± standard deviation of three independent experiments. $^{**}P < 0.01$; $^{***}P < 0.001$.

a biotinylated HAGLR probe and confirmed the pull-down efficiency in AML cells (**Figure 7B**). Next, miRNAs were extracted using a pull-down procedure, and the levels of the eight candidate miRNAs were detected by qRT-PCR. As shown in **Figure 7C**, miR-326 was heavily pulled down by HAGLR.

Furthermore, we noticed that the expression level of miR-326 was low in both patients with AML and cell lines compared to that in normal groups (**Figure 7D**, **7E**). The dual-luciferase reporter gene system showed that miR-326 mimics significantly reduced the expression of Wt HAGLR instead of Mut HAGLR in HL-60 and THP-1 cells (**Figure 7F**). qRT-PCR analysis revealed that silencing HAGLR significantly promoted the expression of miR-326 (**Figure 7G**), whereas miR-326 overexpression clearly decreased HAGLR expression (**Figure 7H**). Overexpression of HAGLR reduced the inhibitory effects of the miR-326 mimic (**Figure 7I**). These results suggest that HAGLR acts as a ceRNA sponge and inhibits miR-326 expression in AML cells.

lncRNA HAGLR sponges miR-326 to upregulate CDKN2A

We predicted the possible mRNAs involved using three algorithms (miRDB, miRTarBase, and TargetScan) (**Figure 8A**), and qRT-PCR validation was performed for the seven target genes that were predicted to be relatively highly expressed in AML and NC. As shown in **Figure 8B**, CDKN2A expression was significantly higher than that in matched healthy controls (**Figure 8C**) and was also higher in THP-1 and HL-60 cells than in other AML cell lines (**Figure 8D**). The dual luciferase reporter gene system showed that miR-326 mimics significantly reduced the expression of CDKN2A with Wt instead of Mut in HL-60 and THP-1 cells (**Figure 8E**). qRT-PCR revealed that the miR-326 mimic inhibited the expression of CDKN2A, but these alterations were reversed by HAGLR overexpression (**Figure 8F**). We used the KEGG pathway and GO to analyze the biological function of HAGLR and signaling pathways (**Figure 8G**, **8H**). These findings demonstrate that HAGLR sponges miR-326 to upregulate CDKN2A expression.

Elesclomol inhibits growth of AML in vitro

Elesclomol is a potent inducer of oxidative stress in cancer cells. To determine the effects of elesclomol on AML cell growth, HL-60 and THP-1 cells were treated with elesclomol. The MTT assay showed that 1, 5, 10 and 20 μm of elesclomol caused a time-dependent, decrease in AML cell growth (**Figure 9A**). Further, HL-60 and THP-1 cells were transfected with si-HAGLR combined with Elesclomo, expression of CDKN2A was dramatically reduced (**Figure 9B**). The si-HAGLR combined with elesclomo significantly inhibited proliferation (**Figure 9C**) and promoted apoptosis *in vitro* (**Figure 9D**). In summary, our data suggested that elesclomol inhibited AML cell growth and promoted apoptosis.

Mechanistic validation of combretastatin si-HAGLR and elesclomol for synergistic therapy of AML in vivo

We also examined the role of combretastatin si-HAGLR and elesclomol in combination therapy *in vivo*. Tumor volume and weight were significantly smaller in the si-HAGLR combined with elesclomol group, whereas they were dramatically increased in the saline group compared to the other groups (**Figure 10A-C**). Ki-67 immunofluorescent staining was used to identify cellular proliferative activity. As shown in **Figure 10D**, there was fewer Ki-67 in the si-HAGLR combined with elesclomol group than in the other groups. H&E staining showed more necrotic areas in the si-HAGLR combined with elesclomol group than in the other groups. Meanwhile, there was strong fluorescence of

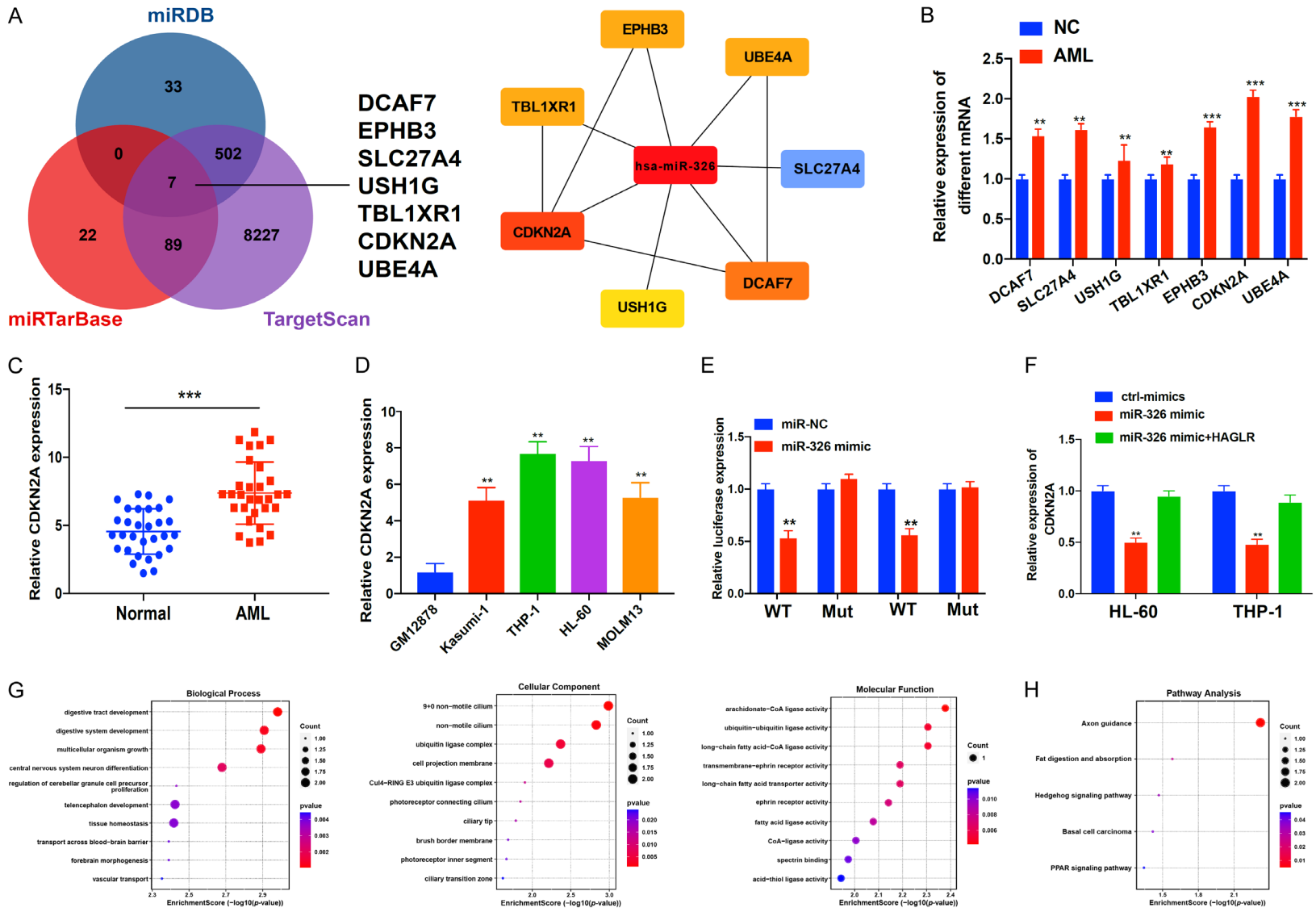

Figure 8. lncRNA HAGLR sponged miR-326 to upregulate CDKN2A. A. Network analysis of miRNA and their target genes by miRDB, miRTarBase and TargetScan. B. The comparative levels of 7 mRNA candidates in AML cells were detected by qRT-PCR. C. CDKN2A expression in the blood samples from 30 sufferers and matched healthy control was examined with qRT-PCR analysis. D. CDKN2A expression in different AML cell lines was determined by qRT-PCR assay. E. Dual-luciferase reporter gene system assay was performed to validate the binding sites of miR-326 and CDKN2A in AML cells. F. Relative levels of CDKN2A in AML cells transfected with miR-326 mimic or miR-326 mimic binds to overexpression HAGLR. G, H. Software R was used to analyze GO biological function and KEGG pathway enrichment. Data are shown as the mean ± standard deviation of three independent experiments. $^{**}P < 0.01$; $^{***}P < 0.001$.

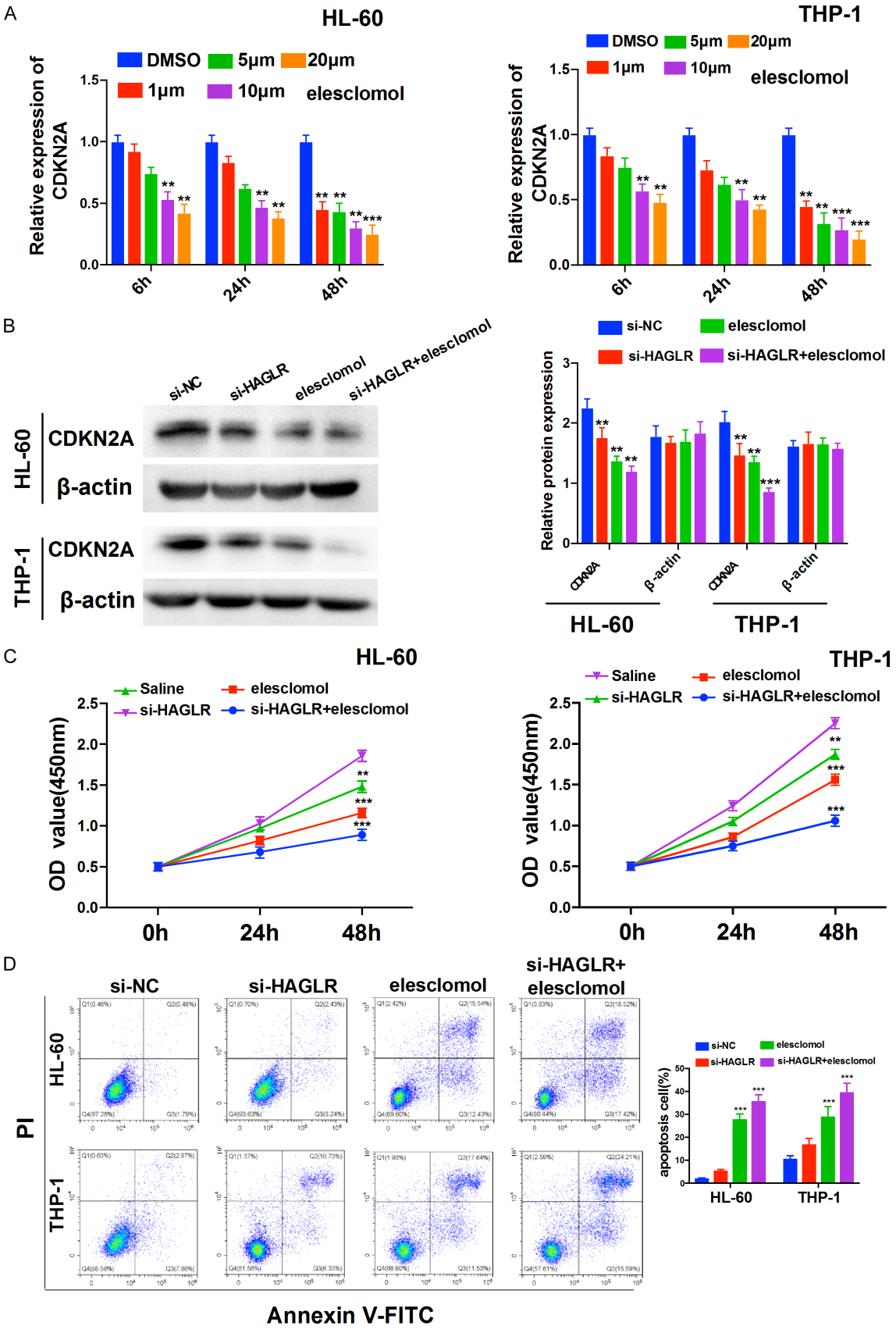
A
HL-60
THP-1
DMSO
5μm
20μm
1μm
10μm
elesclomol
Relative expression of CDKN2A
6h
24h
48h
B
si-NC
si-HAGLR
elesclomol
si-HAGLR+elesclomol
HL-60
THP-1
CDKN2A
β-actin
Relative protein expression
C
Saline
OD value(450nm)
0h
24h
48h
D
si-NC
si-HAGLR
elesclomol
si-HAGLR+ elesclomol
PI
Annexin V-FITC
apoptosis cell(%)

Figure 9. Elesclomol promotes the degradation of CDKN2A and regulates AML cell proliferation and apoptosis. A. qRT-PCR analysis of CDKN2A expression after treated with different doses of elesclomol. B. Relative protein levels of CDKN2A of HL-60 and THP-1 treated with si-NC, si-HAGLR, elesclomol (10 μm), and si-HAGLR+Elesclomol for 24 h, respectively. The quantitation data from immunoblotting analysis were analyzed via ImageJ program. C. The proliferation of HL-60 and THP-1 cells were detected by CCK-8 assays. D. Flow cytometry was employed to identify cell apoptosis of HL-60 and THP-1 cells after 24 h. Data are shown as the mean ± standard deviation of three independent experiments. $^{**}P < 0.01$, $^{***}P < 0.001$.

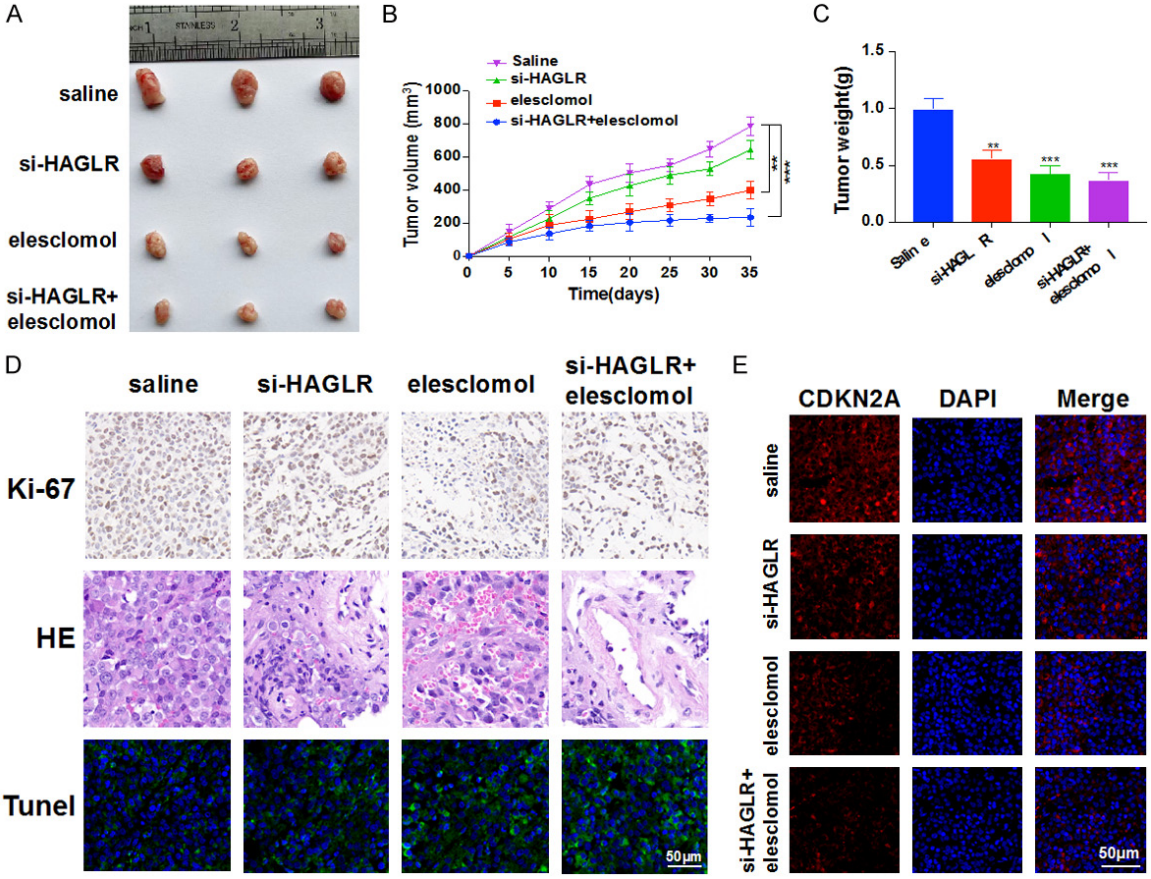

Figure 10. Mechanistic validation of combretastatin si-HAGLR and elesclomol for synergistic therapy of AML *in vivo*. A. Effects of suppression of combretastatin si-HAGLR and elesclomol on tumor volume and tumor weight. B, C. Tumor volume and weight after the sacrifice of all mice on day 34 after treatment of the tested mice with si-NC, si-HAGLR, elesclomol and si-HAGLR+elesclomol, respectively. D. HE and Ki-67 were detected by immunohistochemistry. Tunel (green) were detected by immunofluorescence. Scale bar: 50 μm. E. CDNK2A (red) were detected by immunofluorescence on mouse tumor tissue. Scale bar: 50 μm. Data are shown as the mean ± standard deviation of three independent experiments. $^{**}P < 0.01$, $^{***}P < 0.001$.

TUNEL (green) (**Figure 10D**) and weak fluorescence of CDKN2A (red) (**Figure 10E**) in tumor tissues in the si-HAGLR combined with elesclomol group, in contrast to the other groups. These findings indicated a strong suppressive role of si-HAGLR combined with elesclomol in the proliferation of leukemia cells *in vivo*.

Discussion

AML is a heterogeneous disease characterized by extensive genomic changes and mutations. The therapeutic landscape of AML has undergone a significant transformation because of basic and translational studies, particularly through the use of large-scale genomic assessments to obtain a detailed understanding of the molecular structure of AML. Despite these advancements, primary resistance to initial treatment and disease relapse continue to be significant unmet needs in the treatment of AML. AML is often classified using an approach developed by the World Health Organization (WHO), which is based on an in-depth investiga-

tion of cytochemistry, cytomorphology, genetics, immunophenotypes, and clinical characteristics [22]. The effectiveness of chemotherapy is determined by the cytogenetic and molecular phenotypes of various AML subtypes [23]. More than half of AML patients relapse because their clones are diverse [24, 25]. Furthermore, somatic heterogeneity presents a major barrier to AML therapeutic approaches [26] and it emphasizes the necessity of developing therapeutic alternatives that are both more efficient and specifically targeted.

Programmed cell death involves apoptosis, thermal apoptosis, necrosis, and iron-mediated apoptosis. Cu serves as a vital cofactor for all organisms; however, it becomes toxic if its concentration exceeds the threshold maintained by evolutionarily conserved homeostatic mechanisms. However, the influence of Cu toxicity on AML tumorigenesis is not fully understood. Mechanisms of Cu-induced tumor cell death First, oxidative stress: copper-mediated reduction of Fenton's reaction or antioxidant molecules results in increased ROS levels, subsequently causing mitochondrial dysfunction and accelerated apoptosis; second, proteasome inhibition: copper's interaction with proteasome subunits leads to the accumulation of ubiquitinated proteins; and third, anti-angiogenesis: depleting copper hampers the formation of new blood vessels, further restricting nutrient supply to the tumor tissue [27]. These anticancer mechanisms eventually contribute to the suppression of tumor growth and even cell death. Given its benefits in cancer therapy, the potential biomedical applications of copper warrant extensive investigation. Chemotherapy resistance and nonspecific cytotoxicity are the primary challenges in AML treatment. Anthracyclines (doxorubicin, daunorubicin, epirubicin, and idarubicin) are effective drugs for treating various cancer types, including AML [28]. These well-tolerated and safe agents demonstrate exceptional selectivity and potency against tumor cells, and facilitate antitumor therapy by inducing tumor cell death through apoptosis.

Several studies have shown that modifications in cuproptosis may play a regulatory role in tumorigenesis. Whether cuproptosis modifiers can modify specific lncRNAs, the relationship between cuproptosis and lncRNAs in the maintenance of various cancers, whether cuproptosis modifications of lncRNAs affect tumorigenesis and progression, and whether lncRNAs, as competing endogenous RNAs, are influenced by cuproptosis regulators and thus promote cancer invasion and progression remain to be investigated. Our study showed that surface cuproptosis modifications are specific to lncRNAs, and more attention should be paid to the interaction and function of lncRNAs and cuproptosis modifications to identify potential tumor prognostic biomarkers or therapeutic targets.

In this study, 1255 cuproptosis-associated lncRNAs were identified from the TCGA database to investigate the prognostic effect of cuproptosis-associated lncRNAs. The TCGA database corroborated the prognostic merits of 18 cuproptosis-associated lncRNAs, six of which were utilized to establish cuproptosis-associated lncRNA models to predict OS in patients with AML. Based on the median risk score, patients with AML were subsequently separated into low- and high-risk groups, with the high-risk group experiencing considerably poorer clinical results. Multivariate Cox regression analyses revealed that cuproptosis-associated lncRNA modeling was its own OS risk factor for OS. Receiver operating characteristic (ROC) evaluations demonstrated that the modeling approach outperformed conventional clinical characteristics in predicting AML survival. Our team created a nomograph displaying full agreement between the identified and anticipated OS rates at one, three, and five years. The predicted and observed OS rates at one, three, and five years of age were in good agreement. Risk modeling based on six cuproptosis-associated lncRNAs related to OS in an independent manner exhibited remarkable accuracy, and such predictive modeling methods can determine novel markers for future research.

In clinical practice, pathological staging is an independent factor affecting AML [29]. Nevertheless, patients with AML in the same phase consistently exhibit diverse clinical results, indicating that the current staging system is inaccurate in offering reliable forecasts and in presenting the inhomogeneity of AML. Therefore, potential predictive and treatment markers need to be investigated. The constructed cuproptosis-associated lncRNA model offers a novel approach for predicting the prognosis of patients with AML. The findings offer insights

for subsequent researches on the processes and mechanisms of cuproptosis-modified lncRNAs [30, 31]. In our study, we collected clinical samples to verify the expression of cuproptosis-associated lncRNAs and discovered that cuproptosis-associated lncRNAs were significantly upregulated in AML with poor prognosis, suggesting that cuproptosis-associated lncRNAs might participate in AML development. There are certain flaws in the present research. The biological mechanisms underlying cuproptosis-associated lncRNAs have not been thoroughly elucidated. Therefore, our team will substantiate the accuracy of our modeling method and the biofunctions of cuproptosis-associated lncRNAs through additional experiments in our next work to investigate the roles of lncRNAs and their interactions with cuproptosis-as genes.

In this study, a novel lncRNA, HAGLR/miR-326/CDKN2A, was identified in AML using biological tools. We demonstrated that HAGLR and CDKN2A were upregulated, whereas miR-326 was downregulated in human AML tissues and cells. Moreover, functional experiments performed using si-HAGLR transfection revealed that the proliferation and apoptosis of AML cells were inhibited following the interference of HAGLR, which is consistent with previous reports on the lncRNA HAGLR. In addition, Ma *et al*. found that miR-326 expression was decreased and could act as a tumor suppressor in gastric cancer [32]. This report supported our experimental results on the low expression of miR-326 in AML. Cuproptosis-related prognostic gene CDKN2A was involved in tumor cell growth and drug resistance in human breast cancer [33]. A previous study revealed that the miR-125a-5p/CDKN2A regulatory axis plays a vital role in cervical cancer prognosis [34]. Next, we also revealed the regulatory mechanisms of HAGLR, miR-326 and CDKN2A in AML cells and discovered that the overexpression of HAGLR promoted the CDKN2A expression via being an RNA sponge for miR-326, In short, we concluded that HAGLR upregulated CDKN2A through sponging miR-326, which might be the indispensable mechanism of lncRNA HAGLR-regulated AML progression.

Esclomol, a potential anticancer agent, exhibits antitumor properties by disrupting the cytoskeleton of tumor cells [35] and has been shown to induce oxidative stress in melanoma and leukemia cells, culminating in apoptosis. Esclomol has also been shown to hinder the proliferation of cisplatin-resistant lung cancer cells by augmenting ROS levels [36]. ROS primarily originate from intracellular redox reactions, in which mitochondria serve a crucial function [37]. This aligns with the connection between copper-induced cell death and mitochondrial metabolism. In research on Esclomol-induced cell death, the consensus is that such cell death is mediated by increased ROS levels triggered by various mitochondria-related factors. In a 2013 study conducted in human leukemia K562 cells, copper ions were suggested to be able to oxidize ascorbic acid and react with H_2O_2 to produce more damaging ROS after entering cells via Esclomol transport [38]. Therefore, we hypothesize that Esclomol facilitates copper ion transport and contributes to reduced levels of mitochondria-associated proteins, thereby elevating ROS levels and further inhibiting AML cell proliferation. Our study found reduced CDKN2A expression in immunofluorescence-stained tumor tissues after si-HAGLR binds to elesclomol. The tumor volume and weight decreased, confirming successful antitumor treatment with the combination of drugs. In addition, a significant reduction in tumor cells and an increase in bad tissue were observed after the combination of drugs.

In conclusion, our study offers insight into prognostic forecasts in patients with AML and might facilitate the elucidation of the causal link between cuproptosis and the regulation of lncRNAs. Predictive models exhibited susceptibility in identifying patients with AML who might respond well to immunotherapy. Moreover, our study revealed a synergistic effect between si-HAGLR and elesclomol when used as chemotherapeutic drugs. The apoptosis-enhancing effect of the combined treatment, which was not accompanied by increased killing of normal cells, highlights the therapeutic potential of the components of a more effective drug regimen.

Acknowledgements

This work was supported by the Fundamental Research Funds for Science and Technology Foundation of Guizhou Province (ZK[2021]-013).

Disclosure of conflict of interest

None.

Address correspondence to: Xinhua Luo, Department of Infectious Diseases, Guizhou Provincial People's Hospital, Guiyang 550002, Guizhou, China. Tel: +86-18198262285; E-mail: luoxh09@163.com

References

[1] Binder S, Luciano M and Horejs-Hoeck J. The cytokine network in acute myeloid leukemia (AML): a focus on pro- and anti-inflammatory mediators. Cytokine Growth Factor Rev 2018; 43: 8-15.

[2] Döhner H, Weisdorf DJ and Bloomfield CD. Acute myeloid leukemia. N Engl J Med 2015; 373: 1136-52.

[3] Shah A, Andersson TM, Rachet B, Björkholm M and Lambert PC. Survival and cure of acute myeloid leukaemia in England, 1971-2006: a population-based study. Br J Haematol 2013; 162: 509-16.

[4] De Kouchkovsky I and Abdul-Hay M. 'Acute myeloid leukemia: a comprehensive review and 2016 update'. Blood Cancer J 2016; 6: e441.

[5] Liu H. Emerging agents and regimens for AML. J Hematol Oncol 2021; 14: 49.

[6] Carneiro BA and El-Deiry WS. Targeting apoptosis in cancer therapy. Nat Rev Clin Oncol 2020; 17: 395-417.

[7] Weinlich R, Oberst A, Beere HM and Green DR. Necroptosis in development, inflammation and disease. Nat Rev Mol Cell Biol 2017; 18: 127-36.

[8] Bergsbaken T, Fink SL and Cookson BT. Pyroptosis: host cell death and inflammation. Nat Rev Microbiol 2009; 7: 99-109.

[9] Tsvetkov P, Detappe A, Cai K, Keys HR, Brune Z, Ying W, Thiru P, Reidy M, Kugener G, Rossen J, Kocak M, Kory N, Tsherniak A, Santagata S, Whitesell L, Ghobrial IM, Markley JL, Lindquist S and Golub TR. Mitochondrial metabolism promotes adaptation to proteotoxic stress. Nat Chem Biol 2019; 15: 681-9.

[10] Hasinoff BB, Yadav AA, Patel D and Wu X. The cytotoxicity of the anticancer drug elesclomol is due to oxidative stress indirectly mediated through its complex with Cu(II). J Inorg Biochem 2014; 137: 22-30.

[11] Tardito S, Bassanetti I, Bignardi C, Elviri L, Tegoni M, Mucchino C, Bussolati O, Franchi-Gazzola R and Marchiò L. Copper binding agents acting as copper ionophores lead to caspase inhibition and paraptotic cell death in human cancer cells. J Am Chem Soc 2011; 133: 6235-42.

[12] Cen D, Brayton D, Shahandeh B, Meyskens FL Jr and Farmer PJ. Disulfiram facilitates intracellular Cu uptake and induces apoptosis in human melanoma cells. J Med Chem 2004; 47: 6914-20.

[13] Kirshner JR, He S, Balasubramanyam V, Kepros J, Yang CY, Zhang M, Du Z, Barsoum J and Bertin J. Elesclomol induces cancer cell apoptosis through oxidative stress. Mol Cancer Ther 2008; 7: 2319-27.

[14] Tardito S, Barilli A, Bassanetti I, Tegoni M, Bussolati O, Franchi-Gazzola R, Mucchino C and Marchiò L. Copper-dependent cytotoxicity of 8-hydroxyquinoline derivatives correlates with their hydrophobicity and does not require caspase activation. J Med Chem 2012; 55: 10448-59.

[15] Nagai M, Vo NH, Shin Ogawa L, Chimmanamada D, Inoue T, Chu J, Beaudette-Zlatanova BC, Lu R, Blackman RK, Barsoum J, Koya K and Wada Y. The oncology drug elesclomol selectively transports copper to the mitochondria to induce oxidative stress in cancer cells. Free Radic Biol Med 2012; 52: 2142-50.

[16] Shimada K, Reznik E, Stokes ME, Krishnamoorthy L, Bos PH, Song Y, Quartararo CE, Pagano NC, Carpizo DR, Decarvalho AC, Lo DC and Stockwell BR. Copper-binding small molecule induces oxidative stress and cell-cycle arrest in glioblastoma-patient-derived cells. Cell Chem Biol 2018; 25: 585-94, e7.

[17] Chen D, Cui QC, Yang H and Dou QP. Disulfiram, a clinically used anti-alcoholism drug and copper-binding agent, induces apoptotic cell death in breast cancer cultures and xenografts via inhibition of the proteasome activity. Cancer Res 2006; 66: 10425-33.

[18] Liu N, Huang H, Dou QP and Liu J. Inhibition of 19S proteasome-associated deubiquitinases by metal-containing compounds. Oncoscience 2015; 2: 457-66.

[19] Skrott Z, Mistrik M, Andersen KK, Friis S, Majera D, Gursky J, Ozdian T, Bartkova J, Turi Z, Moudry P, Kraus M, Michalova M, Vaclavkova J, Dzubak P, Vrobel I, Pouckova P, Sedlacek J, Miklovicova A, Kutt A, Li J, Mattova J, Driessen C, Dou QP, Olsen J, Hajduch M, Cvek B, Deshaies RJ and Bartek J. Alcohol-abuse drug disulfiram targets cancer via p97 segregase adaptor NPL4. Nature 2017; 552: 194-9.

[20] Dudekula DB, Panda AC, Grammatikakis I, De S, Abdelmohsen K and Gorospe M. CircInteractome: a web tool for exploring circular RNAs and their interacting proteins and microRNAs. RNA Biol 2016; 13: 34-42.

[21] Jiang P, Gu S, Pan D, Fu J, Sahu A, Hu X, Li Z, Traugh N, Bu X, Li B, Liu J, Freeman GJ, Brown MA, Wucherpfennig KW and Liu XS. Signatures of T cell dysfunction and exclusion predict cancer immunotherapy response. Nat Med 2018; 24: 1550-8.

[22] Arber DA, Orazi A, Hasserjian R, Thiele J, Borowitz MJ, Le Beau MM, Bloomfield CD, Cazzola M and Vardiman JW. The 2016 revision to

the World Health Organization classification of myeloid neoplasms and acute leukemia. Blood 2016; 127: 2391-405.
[23] Estey E and Döhner H. Acute myeloid leukaemia. Lancet 2006; 368: 1894-907.
[24] Ishikawa F, Yoshida S, Saito Y, Hijikata A, Kitamura H, Tanaka S, Nakamura R, Tanaka T, Tomiyama H, Saito N, Fukata M, Miyamoto T, Lyons B, Ohshima K, Uchida N, Taniguchi S, Ohara O, Akashi K, Harada M and Shultz LD. Chemotherapy-resistant human AML stem cells home to and engraft within the bone-marrow endosteal region. Nat Biotechnol 2007; 25: 1315-21.
[25] Ho TC, Lamere M, Stevens BM, Ashton JM, Myers JR, O'dwyer KM, Liesveld JL, Mendler JH, Guzman M, Morrissette JD, Zhao J, Wang ES, Wetzler M, Jordan CT and Becker MW. Evolution of acute myelogenous leukemia stem cell properties after treatment and progression. Blood 2016; 128: 1671-8.
[26] Cancer Genome Atlas Research Network, Ley TJ, Miller C, Ding L, Raphael BJ, Mungall AJ, Robertson A, Hoadley K, Triche TJ Jr, Laird PW, Baty JD, Fulton LL, Fulton R, Heath SE, Kalicki-Veizer J, Kandoth C, Klco JM, Koboldt DC, Kanchi KL, Kulkarni S, Lamprecht TL, Larson DE, Lin L, Lu C, Mclellan MD, Mcmichael JF, Payton J, Schmidt H, Spencer DH, Tomasson MH, Wallis JW, Wartman LD, Watson MA, Welch J, Wendl MC, Ally A, Balasundaram M, Birol I, Butterfield Y, Chiu R, Chu A, Chuah E, Chun HJ, Corbett R, Dhalla N, Guin R, He A, Hirst C, Hirst M, Holt RA, Jones S, Karsan A, Lee D, Li HI, Marra MA, Mayo M, Moore RA, Mungall K, Parker J, Pleasance E, Plettner P, Schein J, Stoll D, Swanson L, Tam A, Thiessen N, Varhol R, Wye N, Zhao Y, Gabriel S, Getz G, Sougnez C, Zou L, Leiserson MD, Vandin F, Wu HT, Applebaum F, Baylin SB, Akbani R, Broom BM, Chen K, Motter TC, Nguyen K, Weinstein JN, Zhang N, Ferguson ML, Adams C, Black A, Bowen J, Gastier-Foster J, Grossman T, Lichtenberg T, Wise L, Davidsen T, Demchok JA, Shaw KR, Sheth M, Sofia HJ, Yang L, Downing JR and Eley G. Genomic and epigenomic landscapes of adult de novo acute myeloid leukemia. N Engl J Med 2013; 368: 2059-74.
[27] Jiang Y, Huo Z, Qi X, Zuo T and Wu Z. Copper-induced tumor cell death mechanisms and antitumor theragnostic applications of copper complexes. Nanomedicine (Lond) 2022; 17: 303-24.
[28] Estey EH. Treatment of acute myeloid leukemia. Haematologica 2009; 94: 10-6.
[29] Bobillo S, Joffe E, Lavery JA, Sermer D, Ghione P, Noy A, Caron PC, Hamilton A, Hamlin PA, Horwitz SM, Kumar A, Matasar MJ, Moskowitz A, Owens CN, Palomba ML, Batlevi CL, Straus D, Von Keudell G, Zelenetz AD, Yahalom J, Dogan A, Seshan VE and Younes A. Clinical characteristics and outcomes of extranodal stage I diffuse large B-cell lymphoma in the rituximab era. Blood 2021; 137: 39-48.
[30] Hou G, Zhao X, Li L, Yang Q, Liu X, Huang C, Lu R, Chen R, Wang Y, Jiang B and Yu J. SUMOylation of YTHDF2 promotes mRNA degradation and cancer progression by increasing its binding affinity with m6A-modified mRNAs. Nucleic Acids Res 2021; 49: 2859-77.
[31] Shang W, Gao Y, Tang Z, Zhang Y and Yang R. The pseudogene Olfr29-ps1 promotes the suppressive function and differentiation of monocytic MDSCs. Cancer Immunol Res 2019; 7: 813-27.
[32] Ma X, Wang G, Fan H, Li Z, Chen W, Xiao J, Ni P, Liu K, Shen K, Wang Y, Xu Z and Yang L. Long noncoding RNA FAM225A promotes the malignant progression of gastric cancer through the miR-326/PADI2 axis. Cell Death Discov 2022; 8: 20.
[33] Lubecka K, Kaufman-Szymczyk A and Fabianowska-Majewska K. Inhibition of breast cancer cell growth by the combination of clofarabine and sulforaphane involves epigenetically mediated CDKN2A upregulation. Nucleosides Nucleotides Nucleic Acids 2018; 37: 280-9.
[34] Wang T, Zhang XD and Hua KQ. A ceRNA network of BBOX1-AS1-hsa-miR-125b-5p/hsa-miR-125a-5p-CDKN2A shows prognostic value in cervical cancer. Taiwan J Obstet Gynecol 2021; 60: 253-61.
[35] Gehrmann M. Drug evaluation: STA-4783--enhancing taxane efficacy by induction of Hsp70. Curr Opin Investig Drugs 2006; 7: 574-80.
[36] Wangpaichitr M, Wu C, You M, Maher JC, Dinh V, Feun LG and Savaraj N. N',N'-dimethyl-N',N'-bis(phenylcarbonothioyl) propanedihydrazide (Elesclomol) selectively kills cisplatin resistant lung cancer cells through reactive oxygen species (ROS). Cancers (Basel) 2009; 1: 23-38.
[37] Sabharwal SS and Schumacker PT. Mitochondrial ROS in cancer: initiators, amplifiers or an Achilles' heel? Nat Rev Cancer 2014; 14: 709-21.
[38] Yadav AA, Patel D, Wu X and Hasinoff BB. Molecular mechanisms of the biological activity of the anticancer drug elesclomol and its complexes with Cu(II), Ni(II) and Pt(II). J Inorg Biochem 2013; 126: 1-6.

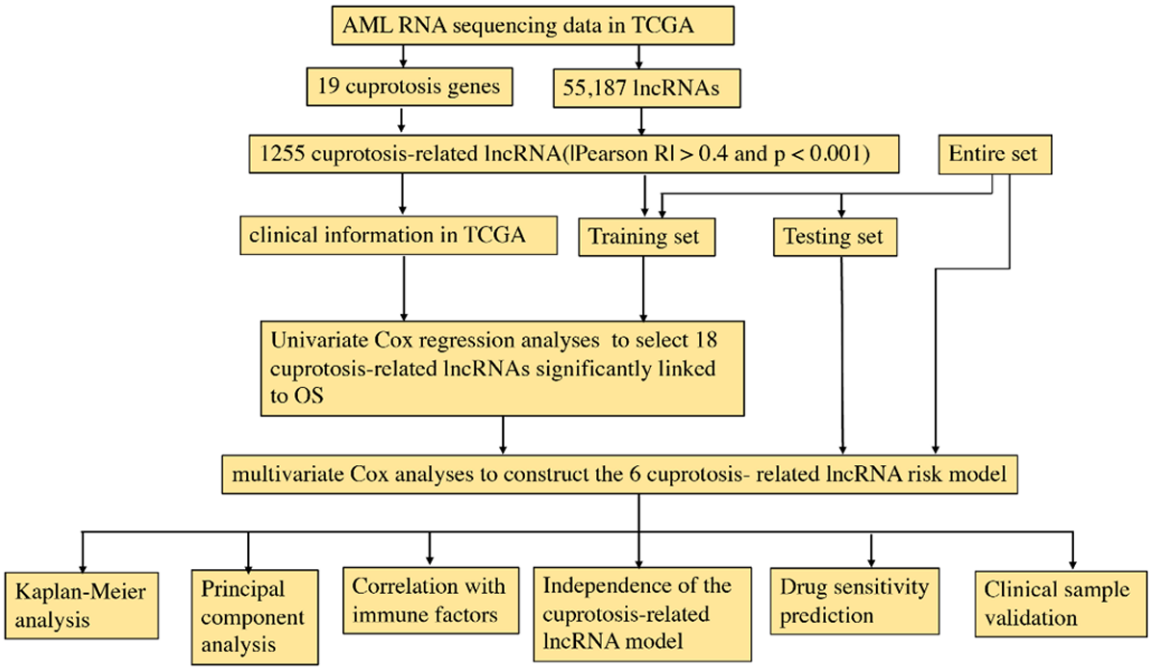

Supplementary Figure 1. Flow chart of the current investigation.

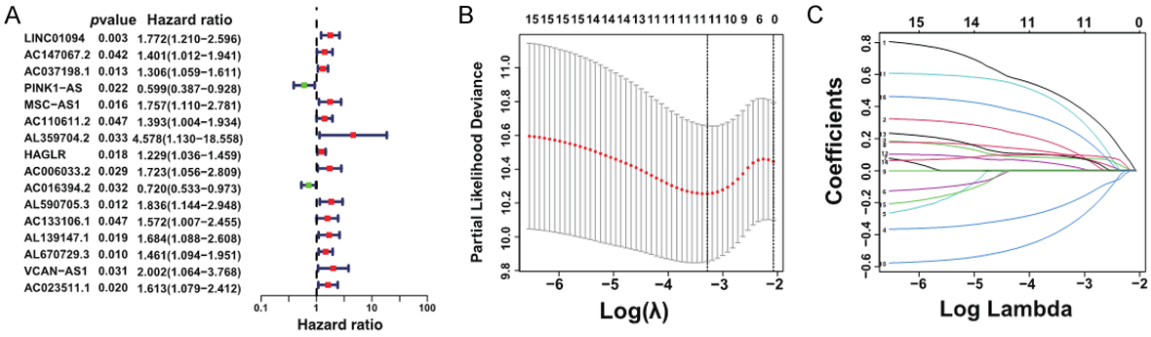

Supplementary Figure 2. Risk modeling for AML sufferers on the foundation of Cuproptosis-associated lncRNAs. A. Univariable Cox regressive analyses unveiled that the chosen lncRNAs were remarkably related to clinical prognoses. B. The adjustment parameters (log λ) of OS-associated protein were chosen to realize the cross-verification of the deviation curve. At the optimal value, vertical imaginary lines were plotted in accordance with the minimum standard and the 1-se standard. C. The profile of the LASSO coefficient for 18 OS-associated lncRNAs as well as an imaginary vertical line was plotted at the value that was determined by 10-fold cross-verification.

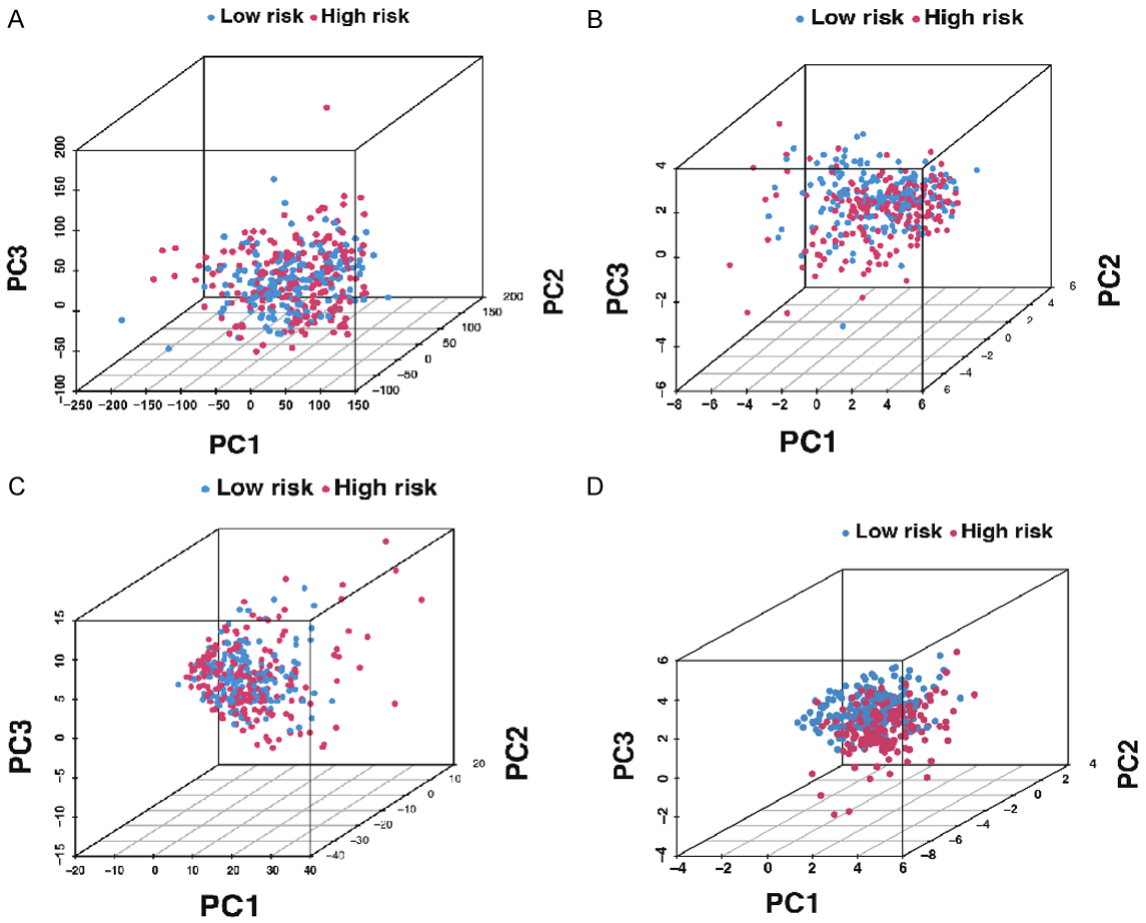

Supplementary Figure 3. PCA between the groups with high- and low-risk. (A) Complete profiles of gene expression, (B) 19 cuproptosis genes, (C) 6 cuproptosis-asociated lncRNAs, and (D) a risk model which is based on the representative profiles of the 6 cuproptosis-associated lncRNAs in the TCGA entire set.

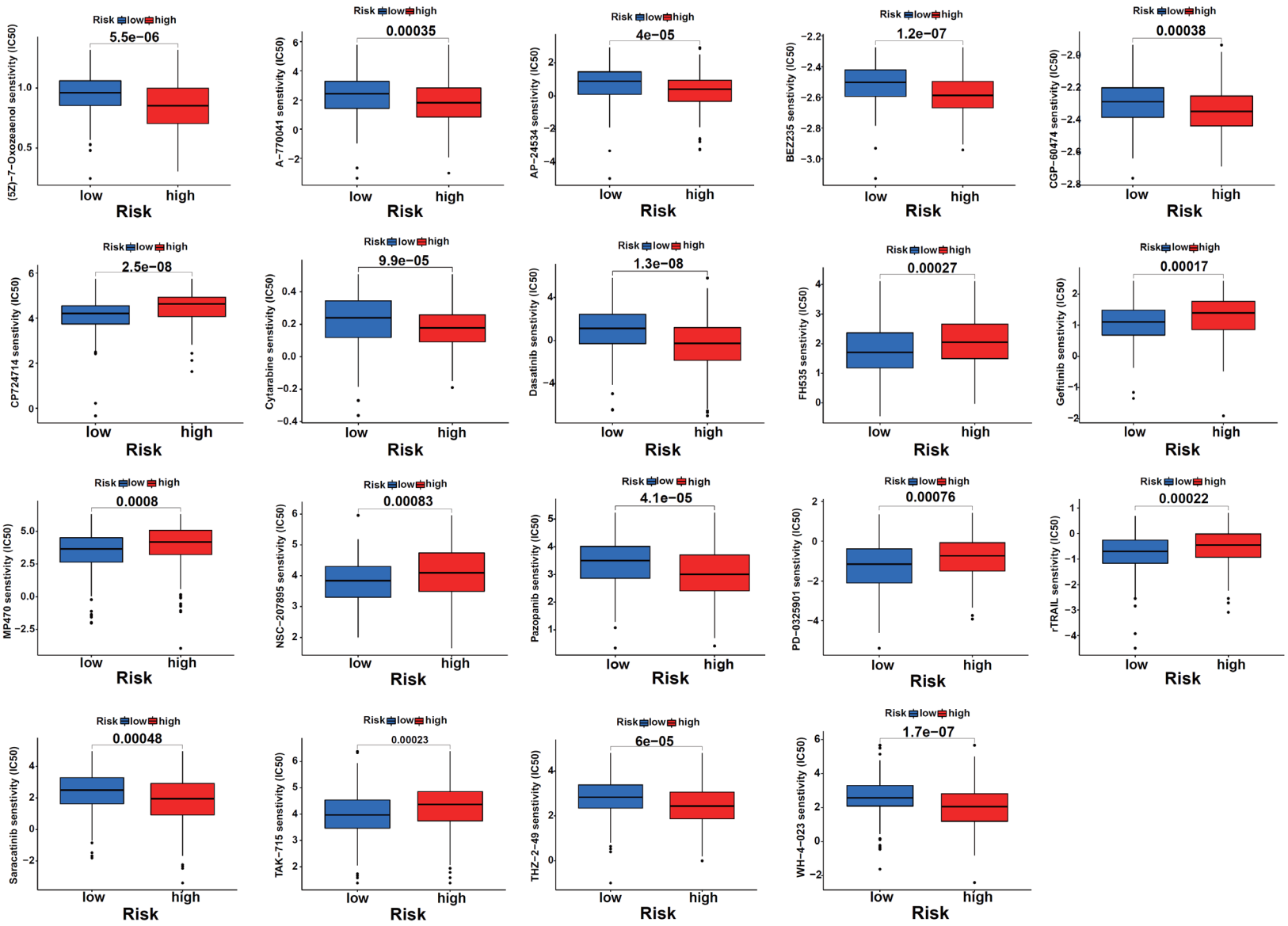

Supplementary Figure 4. Determination of new promising compounds that target the cuproptosis-associated lncRNA model.